



Type-I Graphene/Si Quantum Dot Superlattice for Intermediate Band Applications

Masumeh Sarkhoush^a, Hassan Rasooli Saghai^{b*}, Hadi Soofi^c

^aDepartment of Electrical Engineering, Shabestar Branch, Islamic Azad University, Shabestar, Iran

^bDepartment of Electrical Engineering, Tabriz Branch, Islamic Azad University, Tabriz, Iran

^cFaculty of Electrical and Computer Engineering, University of Tabriz, Tabriz, Iran

Received: 28-09-2022

Accepted: 28-12-2022

Abstract

The most important loss mechanism in single junction solar cells is the inability to convert photons with energies below the bandgap to electricity. Due to quantum confinement, graphene-based quantum dots (QDs) provide a means to create an intermediate band (IB) in the bandgap of semiconductors to absorb sub-bandgap photons. In this work, we introduce a new type-I core/shell-graphene/Si QD for use in all Si-based intermediate band solar cells (IBSCs). Slater-Koster Tight-Binding method is exploited to compute the ground state and the band structure of the graphene/Si QD. The ground state is obtained 0.6 eV above the valence band (VB), which is suitable for creating IB between the conduction band and VB of Si. A superlattice (SL) of this QD is created and the mini-band formation in SL is investigated by varying the inter-dot spacing between QDs. A mini-band with roughly 0.3 eV bandgap is observed in the well-aligned and closely packed SL. This SL is embedded in the intrinsic region of the conventional Si-based solar cell. The mini-band in SL works as an IB in the solar cell and results in increased photon absorption. As a result, carrier generation rate improves from $1.48943 \times 10^{28} \text{ m}^{-3}\text{s}^{-1}$ to $7.94192 \times 10^{28} \text{ m}^{-3}\text{s}^{-1}$ and short circuit current density increases from 211.465 A/m^2 to 364.19 A/m^2 .

Keywords: Graphene; intermediate band; quantum dot; silicon; superlattice

DOI: 10.22059/jsr.2022.349258.1257 DOR: 20.1001.1.25883097.2023.8.1.8.4

1. Introduction

Silicon (Si)-based solar cells are the most valuable commercial photovoltaics due to the great abundance of Si and the well-developed process [1]. Although Si-based solar cells hold the world record in efficiency, the Shockley-Queisser limit states that the maximum theoretical efficiency of Si-based single-junction cells cannot exceed 30% [2]. The intermediate-band solar cell (IBSC) proposed by

Luque and Martí is a concept to overcome the Shockley-Queisser limit. In this concept, an energy band is introduced within the Si bandgap, which is called the intermediate band (IB). This IB provides potential for sequential absorption of sub-bandgap photons that would be lost otherwise. In the past few years, various techniques have been proposed to incorporate the basic principles of IBSC. The most efficient approach is employing of quantum dots (QDs) [3-5].

*Corresponding Author Email Address: h_rasooli@iaut.ac.ir

QD is a nanostructure, whose sizes in all three dimensions are smaller than the De Broglie wavelength of excitons. So, the moving space of electrons becomes smaller than the De Broglie wavelength which results in the confinement effect [6]. This confinement effect induces the quantized and discrete energy levels that are exploited to form IB in the bandgap of a semiconductor [7]. In this field, most of studies have been organized to design IB with multilayer QDs. Rocha. et al have simulated InAsP/InGaP QD for IBSC applications applying Nextnano software in 2019. They have calculated the band structure and wave function of QD by solving the Schrödinger equation and have reported its optical transition energies [8]. Islam. et al have mathematically investigated an IBSC based on PbSe/GaAs QD using Matlab software in 2018. They have reported an optimized high of QD to reach 37.52% conversion efficiency [5]. Hossain. et al have studied the effect of inter-dot spacing between AlInN/GaN QDs on the performance of IBSC utilizing the Schrödinger equation and Kronig–Penney model by Matlab software in 2018. They have found that a 0.3 nm inter-dot spacing results in an optimized width for IB [9]. Villa. et al have designed and fabricated an IBSC based on InAs/AlGaAs QD in 2020. They have focused on enhancement of photon absorption using light trapping techniques and have reached to an increase in the optical path of around 3.5 times, for photon energies in the 0.20–0.35 eV range [10]. Ankh. et al have simulated an IBSC based on InGaAs/GaAs QD with a reduced recombination approach in 2020. They have applied the Schrödinger equation and the Kronig-Penney model to explain the wave function of the electrons in dots and barriers. Their device has shown a low recombination rate 3×10^2 1/cm² with 38.04 mA/cm² short circuit current density (J_{sc}) [11]. Dias. et al have formed IB by growing InAs QDs in InGaP barrier by metal organic vapour phase deposition in 2021. They have investigated the optical characterization of an IBSC based on this QD [12]. Sharan. et al have investigated the effect of position dependent doping on IB generation-recombination rate on InAs/GaAs IBSC 2022. They have used a 1-D drift-diffusion model to obtain the photovoltaic characteristics. These authors have enhanced the conversion efficiency by 0.69% compared to that of un-doped QD IBSCs [13]. Robichaud. et al have investigated the construction of ratchet type IBSC using InGaN quantum dots. They have used a k.p model to calculate the electronic structure and absorptance of superlattice (SL) of InGaN/GaN quantum dots. Optimizing the

dot geometry and alloy fraction allows detailed balance efficiencies up to 42% for their structure [14]. Hu. et al have fabricated type-II Ge/Si QD for IBSC applications using top-down nanofabrication technique in 2013. They have computed the electronic structure of this QD based on the envelope function theory. A SL of this QD with 0.2 nm inter-dot spacing, have increased the efficiency to 45% [1]. Lee. et al have calculated the mini-band structure of Ge/Si QD SL in 2016. These researchers have solved the Schrödinger equation under the Bloch theorem with one-band effective mass approximation [15]. Tsai. et al have designed and simulated an IBSC based on Ge/Si QD in 2017. They have exploited Luque theory derived from the continuity equation to achieve photoelectric characteristics of QD IBSC. They have reported a 27.22% conversion efficiency with bilayer conical QD SL [7].

Owing to unique optical and electrical properties, graphene is a highly considerable material for basic studies [16]. Because of graphene's unique properties and quantum confinement, graphene-based QDs provide a means of creating a sub-bandgap in the bandgap of Si. The high edge/bulk ratio of a graphene edge has a significant influence on the nanoconstraint structures, for example, nanoribbons and quantum dots [17]. However, the absence of bandgap in graphene limits its incorporation in optoelectronic devices. The interaction between graphene and Si surface is strong, leading to the formation of chemical bonds and a large bandgap [18]. Recently, researchers interfaced graphene with silicon to form Schottky junctions that are useful in photo diodes, light harvesters, and solar cells [19].

According to recent studies, graphene based QDs have not been studied for IBSC applications. In this work, for the first time, we introduce a new core/shell QD based on graphene as core and Si as shell of QD, to use in the Si-based IBSCs. We exploit Atomistix-Toolkit (ATK) software to gain energy states and band alignment of our QD. Then we create a SL of the graphene/Si QDs and investigate the mini-band formation in this SL by Slater-Koster (SK) Tight-Banding (TB) method. Finally, to value the potential of the mini-band in the SL as IB, we design an IBSC based on the graphene/Si QD SL and calculate its characteristics by applying Lumerical software. By comparing results with and without QD SL, we observe a considerable improvement.

2. Materials and Methods

We manipulate our simulation using ATK software. We use a (12, 0) Si-Si nanotube with 0.7\AA bond distance to design the shell of our QD. To design the core of QD, we focus on multilayer graphene (MLG). The weak Van Der Waals interlayers coupling in graphene multilayer exert a significant influence on the energy levels, leading to new properties [20]. MLG structure presents a transport bandgap which is generated by the confinement of carriers, mainly due to their own weak anti-localization behavior [21]. Next, we triple the height of the Si-Si nanotube and construct an interface of this nanotube (shell) and MLG (core). Then we shift the shell toward the core and eliminate the carbon atoms which are located outside of the shell. In this way, Si nanotube surrounds MLG. Since Si atoms at the graphene edge prefer sp^2 hybridization, a stable bonding between them is formed. Despite strong Si-C bonds, there are no interactions between graphene layers. Figure 1 shows the atomic structure of the core/shell-graphene/Si QD. Several methods have been developed to fabricate graphene/Si structures. It seems that intercalation is a suitable method for fabricating the proposed QD. Intercalation, where the deposited Si atoms do not stay at the graphene surface but surround graphene layers, may be happen at room temperature [22]. Table 1 presents the material parameters that are used in the design and simulation of the graphene/Si QD.

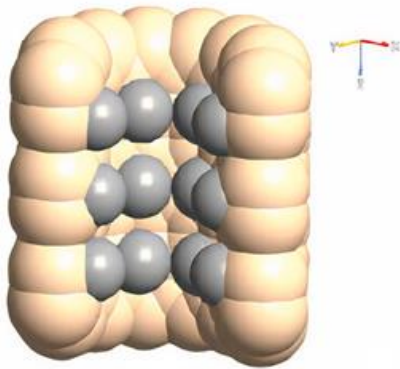


Figure 1. Atomic structure of the core/shell – graphene/Si quantum dot

Table 1. Material parameters used in the simulation of the graphene/Si quantum dot [19].

material	μ_h	μ_e	ϕ_m	x	ϵ	a
Si	1471	479	4.59	4.17	-	5.43
Graphene/Si			4.55	-	-	-
Graphene			-	4.5	5.6053	2.46

A single QD is not able to make a mini-band. The question is that how many neighbours should be included in the Hamiltonian. According to previous studies, including only the first neighbours is not enough for the mini-band creation, the inclusion of second and often the third neighbours is necessary. So we design SL by involving three neighbours as shown in figure 2.

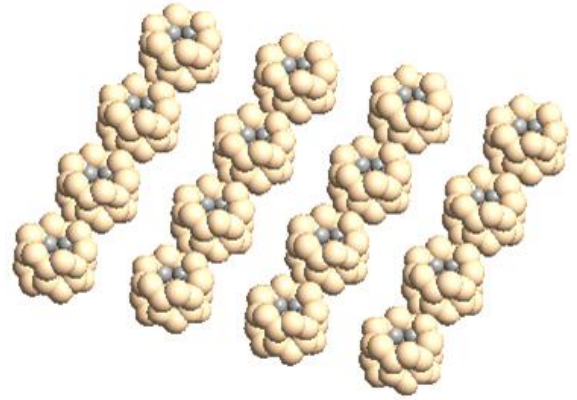


Figure 2. Graphene/Si quantum dot superlattice

3. Computational method

In general, it is difficult to simulate electronic devices in which quantum effects play an important role. Due to advances in nanotechnology, dimensions of electronic devices have been shrunk down to nanoscale. As electrons are trapped in nanoscale regions, the electronic states can be quantized and their behavior can only be described by the Schrödinger equation [23]. Due to strong covalent bonding in the QD, the Schrödinger equation must be solved by TB method. For calculating the electronic band structure of the graphene/Si QD, TB method is performed based on SK approach. The SK-TB formalism or linear combination of atomic orbitals is an extension of Bloch's original method that is primarily used to calculate the band structure and single-particle Bloch states of a material. For large systems containing up to hundreds of atoms, the density function theory (DFT) is used to find the true ground state density and ground state energy of an interaction system without explicitly calculating the many-electron wave function. This semi-empirical method shows all the correct symmetry properties of the energy bands and provides a solution for the single-particle Schrödinger equation at each sampling k-points in the Irreducible Brillouin zone (IBZ) [24].

Equation (1) represents the Schrödinger equation:

$$\left[-\frac{\hbar^2}{2m}\nabla^2\Psi_i(r)+V(r)\Psi_i(r) \right] = E_i\Psi_i(r) \quad (1)$$

where \hbar , m , V , Ψ , and E are the Plank constant, electron mass, potential energy, the wave function, and eigenvalues of energy, respectively [25]. Instead of solving the single-particle Schrödinger equation for each electron, it can be solved in a unit cell that describes the periodicity of the structure. The Fourier transform transfers the unit cell to IBZ in reciprocal space. Figure 3 depicts the unit cell and first IBZ of the graphene/Si QD SL.

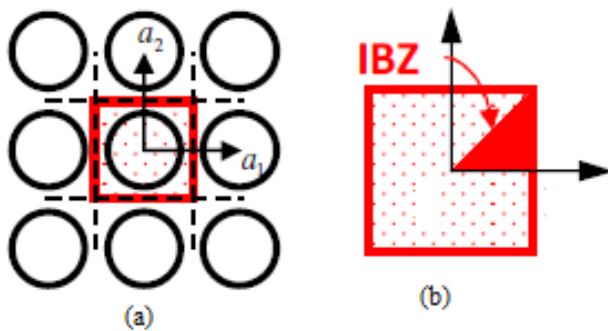


Figure 3(a). The unit cell, (b). first irreducible brillouin zone of graphene/Si quantum dot superlattice.

In the first IBZ, the wave function and potential energy can be written as periodic functions:

$$\Psi(\vec{r}) = \sum_k \Psi_k e^{i\vec{k}\cdot\vec{r}} \quad (2)$$

$$V(\vec{r}) = \sum_{k'} V_{k'} e^{i\vec{k}'\cdot\vec{r}} \quad (3)$$

where k is the wave vector and r denotes the position of particles. The solution of equation (1) by considering equation (2) and equation (3) results in equation (4):

$$\sum_k e^{i\vec{k}\cdot\vec{r}} \left[\left(-\frac{\hbar^2}{2m}\nabla^2 - E \right) \Psi_k + \sum_{k'} V_{k'} \Psi_{k-k'} \right] = 0 \quad (4)$$

For this equation to be valid for every r , the expression in the bracket, which is independent of r , must be equal to zero for every k . Under this condition, a solution to the Schrödinger equation is a

superposition of plane waves whose wave vectors differ only by reciprocal lattice vectors. This solution is presented in equation (5):

$$\Psi(r) = \sum_k C_{k-K} e^{i(K-K')\cdot r} = u(r) e^{i\vec{k}\cdot r} \quad (5)$$

where $u(r)$ is a function determined by the material properties and repeated in every unit cell. Reciprocal function of $u(r)$ is Bloch function which is shown by Φ [26].

If there are n wave vectors considered in every unit cell and there are N unit cells in a crystal lattice, whose position are denoted by R , then the wave functions will be as equation (6):

$$\Psi_j(\vec{k}, \vec{r}) = \frac{1}{\sqrt{N}} \sum_{l=1}^N e^{i\vec{k}\cdot\vec{r}_l} \Phi_j(\vec{r} - \vec{R}_l) \quad (6)$$

If every band is related to one atomic energy level and there are no wave functions overlapping, the wave functions will be obtained by equation (6). In structures such as the graphene/Si QD SL that orbitals from different atoms participate in the formation of the energy band, the wave functions can be computed by equation (7):

$$\Psi_1(\vec{k}, \vec{r}) = \sum_{j=1}^n C_{1,j}(\vec{k}) \Phi_j(\vec{k}, \vec{r}) \quad (7)$$

where c is the weight coefficients and is calculated by solving equation (8):

$$\sum_{n,i} \left(H_{ni,mj} - E(k) \delta_{nm} \delta_{ij} \right) C_{mj}(k) = 0 \quad (8)$$

where the δ -functions enter by neglecting the orbital overlap on different atomic sites and H is the Hamiltonian matrix. δ and H are computed through equation (9) and equation (10) respectively.

$$\int \Psi_{i\alpha}^*(r - R_m - r_i) \Psi_{j\beta}(r - R_n - r_j) d^3r = \delta_{ij} \delta_{mn} \quad (9)$$

$$H_{ij} = \Phi_i |H| \Phi_j \quad (10)$$

By obtaining the characters of the Hamiltonian matrix the equation (9) changes to equation (11):

$$[H]C_i = E_i(\vec{k})[S]C_i \quad (11)$$

where S is the overlap matrixes and can be obtained through equation (12) [27]:

$$S_{ij} = \Phi_i | \Phi_j \quad (12)$$

A unit cell that describes the periodicity of SL is defined to reduce the sampling size of k -points for simulation. A 10×10 k -point sampling grid, cutoff energy of 160 Ry, the Hamiltonian matrix elements that are related to the orbitals which participate in bonding between atoms, and periodic boundary conditions are considered performing these calculations.

4. Results & Discussion

A single QD has an atom-like energy band alignment. It means that the energy levels of a single QD are discrete levels. The levels that have lower energies than the conduction band (CB) edge of the host material are called the bound states, and the levels with higher energies than the CB edge of host material are called virtual bound states. The bound states are usually named by the quantum numbers in the x , y , and z dimensions, respectively, e.g. (1,1,1) and (2,2,1). The bound state with the quantum number (1,1,1) is called the ground state, and it constitutes the IB [28]. To create IB, the optimum ground state in a QD should be 0.9 eV above the valance band (VB) [29]. The simulation results reveal a 0.6 eV ground state above VB for the graphene/Si QD with 3 layers of graphene. It is important to have the IB energy level at 1/3 or 2/3 of the bandgap for equalizing IB photocurrents [28]. Due to the zero bandgap of graphene, the effective bandgap of the graphene/Si QD will decrease if the number of graphene layers increases. So the number of graphene layers must not exceed 3.

Interaction of graphene and Si atoms at their interface results in strain. It has been verified that strain can considerably alter local band edge, which results in band offset. This band offset in heterojunction structures can be calculated by Anderson's rule. If the vacuum levels of constituents are not equal, the CB offset (ΔE_c) will be equal to their affinity's difference [30, 31]. So according to material properties which are reported in table 1, ΔE_c in graphene/Si QD is 0.33 eV.

In graphene/Si QD, the energy level of CB of core is lower than the energy level of CB of shell and the energy level of VB of core is higher than the energy level of VB of shell. As a result, the band layout of this QD is a contravariant alignment which refers to type-I QD. Figure 4 demonstrates energy band alignment for the graphene/Si QD. The blue line is VB edge, the violet line is CB edge, and the black lines are the quantized energy levels for CB and VB electrons inside QD.

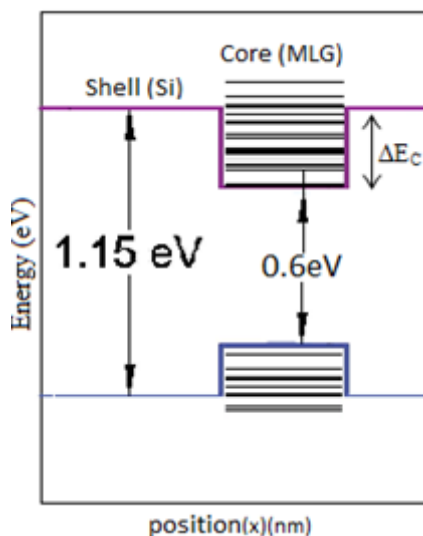


Figure 4. The calculated band alignment for the graphene/Si quantum dot.

Type-I QD traps simultaneously electrons and holes that results in confinement energy levels [32]. So the band state energy level for a single QD is a discrete band state due to the confined quantum levels. It means that a single QD is unable to make the mini-band. In a well-ordered QD SL, QDs interact with neighbour QDs. These interactions broaden the discrete quantum levels which are confined in single QD to form finite-width mini-bands [15]. Figure 5(a) shows the band dispersion relation of the graphene/Si QD SL with a 0.8 nm inter-dot spacing between QDs. For the band dispersion calculation, k varies along the edges of the first IBZ. As it is shown, when inter-dot spacing is 8 nm, there is no interaction among QDs and SL behaves like a single QD. If the inter-dot spacing decreases, the density of QDs increases and then their wave functions spread into neighbours and couple with each other, resulting in the formation of the mini-band. The mini-band formation phenomenon in a well-aligned and closely packed SL is shown in figure 5(b).

To investigate the filling of energy levels by electrons, the density of state (DOS) must be studied. DOS is essentially the number of different states at a particular energy level that electrons are allowed to occupy. It is mathematically represented as a distribution by a probability density function. It is also useful for recognizing of the mini-band's width, which is formed in QDs SL. Figure 6 demonstrates DOS of SL with roughly 0.3 eV bandgap.

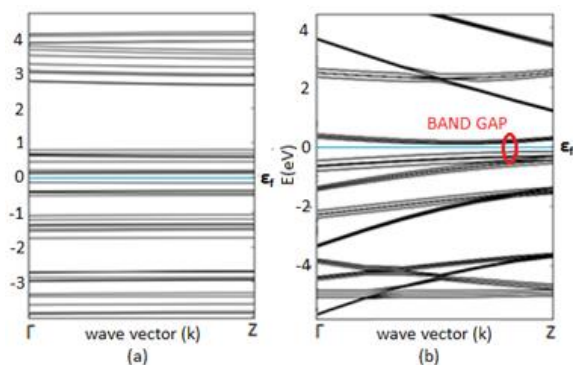


Figure 5. The band structure in k space along wave vector for the graphene/Si quantum dot superlattice (a): with an 8 nm inter-dot spacing; (b): for closely packed superlattice

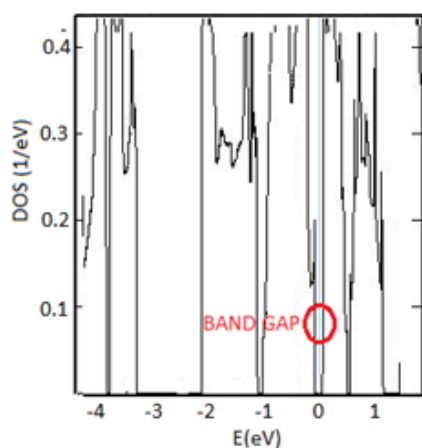


Figure 6. The density of states for closely packed graphene/Si quantum dot superlattice

To investigate the effect of the graphene/Si QD SL on the performance of the Si-based solar cell, we design and simulate a Si-based solar cell using Lumerical software. Then, to design the IBSC, we embed the graphene/Si QD SL in the active layer between p-type and n-type regions. Table 2 presents the model geometry, which is used to design and simulation of the solar cells. This geometry is based on data which is provided on Lumerical software site [33].

Table 2. Model geometry used in the simulation [33].

layer	material	Thickness (um)	Reflective index
AR	-	0.07	2.05
Active layer	Si	3	-
Electrode	Al	0.5	-
QD SL	Graphene/Si	0.02	-

Figure 7 depicts the structure of IBSC based on the graphene/Si QD SL. we compute J_{sc} and carrier generation rate (G) of the solar cell with and without QD SL. In the simulation, the solar cell structures are illuminated by a light source with a spectral range of 0.3-5 μm . The periodic and PML boundary conditions are chosen in X and Y directions, respectively. Using nanostructures such as QDs often causes an open-circuit voltage drop which is observed when sub-bandgap states are introduced [34]. This drop denotes strong Auger recombination. In addition, the nonradiative recombination associated with the sub-bandgap between IB and CB is expected to be large. So Auger and non-radiative recombination are considered in the simulation process. The solar generation rate analyzer, a functional module provided by Lumerical, is exploited to compute the electron-hole generation rate. The generation and recombination of carriers are balanced by continuity equation and results in the diffusion current. Simultaneously, Poisson's equation represents the variations in the electrostatic potential which causes the drift current. Finally, the electron current density in CB and the hole current density in VB are given by drift-diffusion equation.

As it is shown in figure 8, when QD SL is embedded in the active layer of the Si-based solar cell, the mini-band works as IB and G increases significantly. In comparison with the conventional Si-based solar cell, which records $G=1.48943 \times 10^{28} \text{ m}^{-3}\text{s}^{-1}$, the graphene/Si QD IBSC with 2 layers of QDs presents $G=7.94192 \times 10^{28} \text{ m}^{-3}\text{s}^{-1}$.

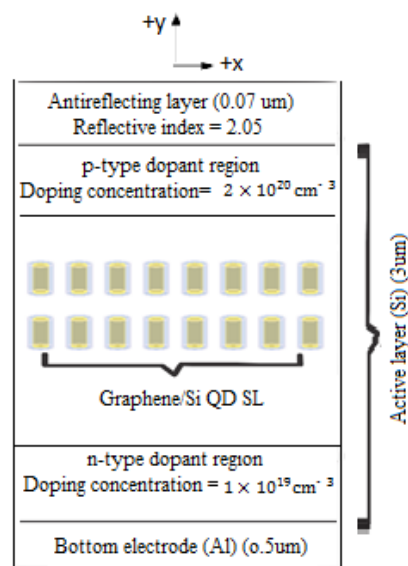


Figure 7. Base structure of graphene/Si quantum dot intermediate band solar cell

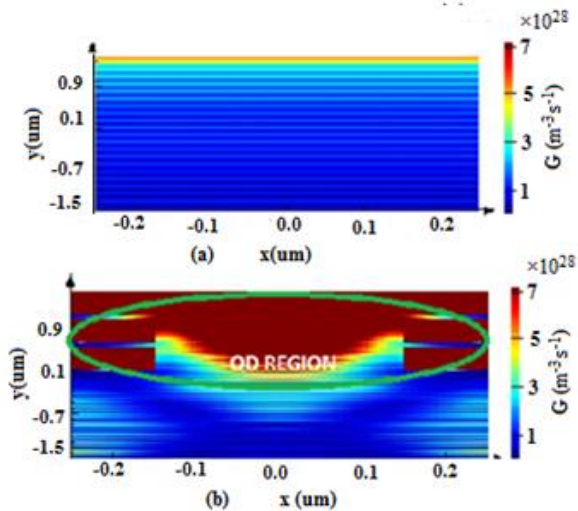


Figure 8. Generation rate (a) for Si-based solar cell; (b) graphene/Si quantum dot intermediate band solar cell.

IB splits the total bandgap of the active layer (E_G) into two sub-bandgaps. These sub-bandgaps absorb photons with energy less than E_G . This process allows for increased photon absorption via the two-step photon absorption from VB to IB and from IB to CB. The enhancement of absorption in IBSC in comparison with the Si-based solar cell is shown in figure 9.

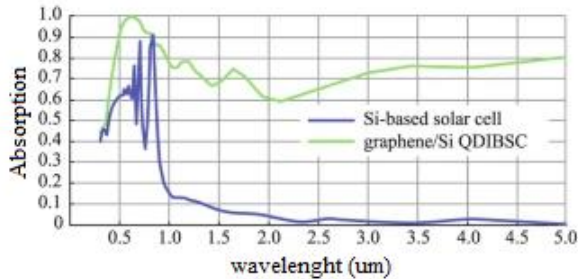


Figure 9. Comparison of the absorption of Si-based solar cell and graphene/Si quantum dot intermediate band solar cell.

The absorption of sub-bandgap photons results in an additional photocurrent. Indeed, the embedding of the graphene/Si QD SL helps to increase the photo-generated current as expected. J_{sc} is calculated 211.465 A/m² for Si-based solar cell without QD SL. By embedding the first layer of QDs, J_{sc} increases to 245.192 A/m². Adding the second layer of QDs, results in a considerable enhancement. J_{sc} of IBSC based on two-layer graphene/Si QDs is estimated 364.193 A/m².

5. Conclusions

In conclusion, a new type-I core/shell-graphene/Si QD is introduced to use in all Si-based IBSCs. The ground state of QD is computed 0.6 eV above VB applying SK-TB method. This result confirms the potential of QD to create IB. A well-aligned and closely packed SL of QDs forms a mini-band with roughly 0.3 eV bandgap. This mini-band is exploited as IB in the active layer of the conventional Si-based solar cell. The IB splits the total bandgap of Si into two sub-bandgaps. As a result, photons with energy below the bandgap of Si are absorbed via the two-photon absorption process, from VB to IB and from IB to CB. Due to significant improvement in absorption, G and J_{sc} increase considerably. In comparison with the conventional Si-based solar cell which records J_{sc} =211.465 A/m² and G =1.48943×10²⁸ m⁻³s⁻¹, the graphene/Si QD IBSC with 2 layers of QDs presents J_{sc} =364.19 A/m² and G =7.94192×10²⁸ m⁻³s⁻¹.

Nomenclature

Si	Silicon
IBSC	Intermediate band solar cell
IB	Intermediate band
QD	Quantum dot
eV	Electron volt
J_{sc}	Short circuit current density (mA/cm ²)
ATK	Atomistix toolkit software
SL	Super lattice
SK	Slater-koster method
TB	Tight-binding method
G	Carrier generation rate (m ⁻³ s ⁻¹)
MLG	Multilayer graphene
μ_e	Electron mobility (cm ² /V.s)
μ_h	Hole mobility (cm ² /V.s)
ϕ_m	Work function (eV)
x	Electron affinity (eV)
ϵ	Dielectric constant
a	Lattice constant (Å)
DFT	Density functional theory
h	Plank constant
m	Electron mass
V	Potential energy
ψ	Wave function
E	Eigenvalues of energy
IBZ	Irreducible Brillouin zone
k	Wave vector
r	Position of particles
u(r)	Function of material properties
ϕ	Bloch function
n	Number of wave vectors
N	Number of unit cells
R	Position of unit cells
c	Weight coefficients
δ	Function of neglecting orbital overlap

H	Hamiltonian matrix
S	Overlap matrix
VB	Valance band
CB	Conduction band
ΔE_c	Conduction band offset
DOS	Density of states
AR	Anti-reflecting layer
E_G	Bandgap

References:

- Hu, W., M.E. Fauzi, M. Igarashi, A. Higo, M.-Y. Lee, Y. Li, N. Usami, and S. Samukawa.(2013). Type-II Ge/Si quantum dot superlattice for intermediate-band solar cell applications. in 2013 IEEE 39th Photovoltaic Specialists Conference (PVSC). IEEE.
- Fioretti, A.N., M. Boccard, R. Monnard, and C. Ballif.(2019). Low-temperature p n -type microcrystalline silicon as carrier selective contact for silicon heterojunction solar cells. IEEE Journal of Photovoltaics. **9**(5): p. 1158-1165.
- Collazos, L.J., M.M. Al Huwayz, R. Jakomin, D.N. Micha, L.D. Pinto, R.M. Kawabata, M.P. Pires, M. Henini, and P.L. Souza.(2021). The role of defects on the performance of quantum dot intermediate band solar cells. IEEE Journal of Photovoltaics. **11**(4): p. 1022-1031.
- Delamarre, A., D. Suchet, N. Cavassilas, Y. Okada, M. Sugiyama, and J.-F. Guillemoles.(2018). An electronic ratchet is required in nanostructured intermediate-band solar cells. IEEE Journal of Photovoltaics. **8**(6): p. 1553-1559.
- Islam, A., A. Das, N. Sarkar, M. Matin, and N. Amin.(2018). Numerical Analysis of PbSe/GaAs Quantum Dot Intermediate Band Solar Cell (QDIBSC). in 2018 International Conference on Computer, Communication, Chemical, Material and Electronic Engineering (IC4ME2). IEEE.
- Dong, B., S. Guo, A. Afanasev, and M. Zaghoul.(2016). Simulations of properties of quantum dots and high-efficiency GaAs solar cells. in 2016 IEEE 43rd Photovoltaic Specialists Conference (PVSC). IEEE.
- Tsai, Y.-C., M.-Y. Lee, Y. Li, and S. Samukawa.(2017). Design and simulation of intermediate band solar cell with ultradense type-II multilayer Ge/Si quantum dot superlattice. IEEE Transactions on Electron Devices. **64**(11): p. 4547-4553.
- Rocha, B., R. Jakomin, R. Kawabata, L. Dornelas, M. Pires, and P. Souza.(2019). Transition Energy Calculations of Type II In (As) P/InGaP Quantum Dots for Intermediate Band Solar Cells. in 2019 34th Symposium on Microelectronics Technology and Devices (SBMicro). IEEE.
- Hossain, M.J., S. Roy, M.S. Hossain, and M. Moznuzzaman.(2018). Analytical modeling of AlInN/GaN quantum dot intermediate band solar cell. in 2018 International Conference on Innovation in Engineering and Technology (ICIET). IEEE.
- Villa, J., I. Ramiro, J.M. Ripalda, I. Tobías, P. García-Linares, E. Antolín, and A. Martí.(2020). Contribution to the study of sub-bandgap photon absorption in quantum dot InAs/AlGaAs intermediate band solar cells. IEEE Journal of Photovoltaics. **11**(2): p. 420-428.
- Ankhi, A.I., M.R. Islam, M.T. Hasan, and E. Hossain.(2020). Projected Performance of InGaAs/GaAs Quantum Dot Solar Cells: Effects of Cap and Passivation Layers. IEEE Access. **8**: p. 212339-212350.
- de Paula Dias, C., E.C. Weiner, R.M.S. Kawabata, R. Jakomin, P.L. Souza, and M.P. Pires.(2021). Optical Characterization of InAs/InGaP Intermediate Band Solar Cells. in 2021 35th Symposium on Microelectronics Technology and Devices (SBMicro). IEEE.
- Sharan, A. and J. Kumar.(2022). Effect of Position-Dependent Doping on Intermediate Band Generation-Recombination Rate in InAs/GaAs Quantum Dot Solar Cell. IEEE Transactions on Nanotechnology. **21**: p. 151-157.
- Robichaud, L. and J.J. Krich.(2022). Ingan quantum dot superlattices as ratchet band solar cells. IEEE Journal of Photovoltaics. **12**(2): p. 474-482.
- Lee, M.-Y., Y.-C. Tsai, Y. Li, and S. Samukawa.(2016). Numerical simulation of physical and electrical characteristics of Ge/Si quantum dots based intermediate band solar cell. in 2016 IEEE 16th International Conference on Nanotechnology (IEEE-NANO). IEEE.

16. Mahmoudi, T., Y. Wang, and Y.-B. Hahn.(2018). Graphene and its derivatives for solar cells application. *Nano Energy*. **47**: p. 51-65.
17. Chen, Q., A.W. Robertson, K. He, C. Gong, E. Yoon, A.I. Kirkland, G.-D. Lee, and J.H. Warner.(2016). Elongated silicon–carbon bonds at graphene edges. *ACS nano*. **10**(1): p. 142-149.
18. Javvaji, B., B.M. Shenoy, D.R. Mahapatra, A. Ravikumar, G. Hegde, and M. Rizwan.(2017). Stable configurations of graphene on silicon. *Applied Surface Science*. **414**: p. 25-33.
19. Arefinia, Z. and A. Asgari.(2017). Optimization study of a novel few-layer graphene/silicon quantum dots/silicon heterojunction solar cell through opto-electrical modeling. *IEEE Journal of Quantum Electronics*. **54**(1): p. 1-6.
20. Mirzakhani, M.(2017). Electronic properties and energy levels of graphene quantum dots, University of Antwerp
21. Lin, I.-T. and J.-M. Liu.(2013). Terahertz frequency-dependent carrier scattering rate and mobility of monolayer and AA-stacked multilayer graphene. *IEEE Journal of Selected Topics in Quantum Electronics*. **20**(1): p. 122-129.
22. Daukiya, L., M.N. Nair, M. Cranney, F. Vonau, S. Hajjar-Garreau, D. Aubel, and L. Simon.(2019). Functionalization of 2D materials by intercalation. *Progress in Surface Science*. **94**(1): p. 1-20.
23. Xiang, C., F. Kong, K. Li, and M. Liu.(2017). A high-order symplectic FDTD scheme for the Maxwell-Schrodinger system. *IEEE Journal of Quantum Electronics*. **54**(1): p. 1-8.
24. Junaid, M. and G. Witjaksono.(2019). Analysis of band gap in AA and Ab stacked bilayer graphene by Hamiltonian tight binding method. in 2019 IEEE International Conference on Sensors and Nanotechnology. IEEE.
25. Papaconstantopoulos, D. and M. Mehl.(2003). The Slater–Koster tight-binding method: a computationally efficient and accurate approach. *Journal of Physics: Condensed Matter*. **15**(10): p. R413.
26. Sun, Y., S.E. Thompson, and T. Nishida,(2009). Strain effect in semiconductors: theory and device applications. 2009: Springer Science & Business Media.
27. Dresselhaus, G., M.S. Dresselhaus, and R. Saito,(1998). Physical properties of carbon nanotubes. 1998: World scientific.
28. Kiziloglu, V., T.S. Navruz, and M. Saritas.(2018). Size Dependent Intermediate Band Energy Levels and Absorption of Bound States in Box Shaped Quantum Dots. in 2018 International Conference on Photovoltaic Science and Technologies (PVCon). IEEE.
29. Hellstroem, S. and S.M. Hubbard.(2014). Drift-diffusion simulations of InAs/AlAsSb quantum dot intermediate-band solar cells. in 2014 IEEE 40th Photovoltaic Specialist Conference (PVSC). IEEE.
30. Chaves, A., J.G. Azadani, H. Alsalman, D. Da Costa, R. Frisenda, A. Chaves, S.H. Song, Y.D. Kim, D. He, and J. Zhou.(2020). Bandgap engineering of two-dimensional semiconductor materials. *npj 2D Materials and Applications*. **4**(1): p. 1-21.
31. Afanas' ev, V.V.(2014). Electron band alignment at interfaces of semiconductors with insulating oxides: An internal photoemission study. *Advances in Condensed Matter Physics*. **2014**.
32. Nandan, Y. and M.S. Mehata.(2019). Wavefunction engineering of type-I/type-II excitons of CdSe/CdS core-shell quantum dots. *Scientific reports*. **9**(1): p. 1-11.
33. .www.kb.lumerical.com
34. Zhu, L., H. Akiyama, and Y. Kanemitsu.(2018). Intrinsic and extrinsic drops in open-circuit voltage and conversion efficiency in solar cells with quantum dots embedded in host materials. *Scientific reports*. **8**(1): p. 1-12.